

Article

Analysis of Photosynthetic Differences of Rice Germplasm in Southeast Asia Based on Leaf-Tissue Structure, Physiology, and iTRAQ

Xiaoli Zhang ^{1,†}, Maoyan Tang ^{1,†}, Hui Wang ², Wei Tao ³, Qiang Wang ¹, Lei Chen ¹ , Guoqing Gao ¹, Ronghua Lv ³ and Tianfeng Liang ^{1,*}

¹ Guangxi Key Laboratory of Rice Genetics and Breeding, Rice Research Institute, Guangxi Academy of Agricultural Sciences, Nanning 530007, China

² Agricultural Science and Technology Information Research Institute, Guangxi Academy of Agricultural Sciences, Nanning 530007, China

³ Guangxi Academy of Agricultural Sciences, Nanning 530007, China

* Correspondence: tfliang@gxaas.net

† These authors contributed equally to this work.

Abstract: Photosynthesis is responsible for 90–95% of organic matter in crop yield. The light energy utilization rate of high-yielding rice varieties is 1.0–1.5%, but the ideal value is about 3–5%. Yield can be further improved by improving photosynthetic function. Through the initial screening and re-screening of 220 Southeast Asian germplasm resources, we found that the net photosynthetic rate of Southeast Asian germplasm resource C1 was $36.96 \mu\text{mol m}^{-2} \text{S}^{-1}$, which is close to that of C₄ plant maize and 3.26 times higher than that of Southeast Asian germplasm resource G164 at $11.26 \mu\text{mol m}^{-2} \text{S}^{-1}$. Using C1 and G164 as materials, we compared the tissue structure, chloroplast ultrastructure, photosynthetic physiological indicators, and proteomics of sword leaves to determine the factors affecting photosynthetic function. Compared with G164, C1 exhibited increased number of vascular bundles, increased stomatal size and density, more abundant and neatly arranged chloroplasts and thylakoid grana, and higher chlorophyll fluorescence parameters. The activities and contents of the key photosynthetic enzyme Rubisco were higher in C1 than in G164. The two germplasm resources were subjected to iTRAQ analysis, and the results showed that compared with C1, nine proteins were down-regulated and one protein was up-regulated and associated with photosynthetic electron transport in G164; a total of 17 differential proteins were associated with CO₂ fixation, and nine were up-regulated and eight differential proteins were down-regulated in G164. The identified genes encode proteins in the photosynthesis and carbon fixation pathways, and the changes in gene expression were verified by real-time qPCR. The gene expression patterns were consistent with the protein expression patterns. The results suggest that most differential proteins are involved in electron transfer from PSII to PSI and in the CO₂ fixation pathway, and increasing the levels of such proteins can effectively enhance the photosynthetic efficiency. C1 can be used as a donor material for selection of high light efficiency varieties and in-depth photosynthesis studies.

Keywords: rice; leaf structure; photosynthesis; iTRAQ; proteomics



Citation: Zhang, X.; Tang, M.; Wang, H.; Tao, W.; Wang, Q.; Chen, L.; Gao, G.; Lv, R.; Liang, T. Analysis of Photosynthetic Differences of Rice Germplasm in Southeast Asia Based on Leaf-Tissue Structure, Physiology, and iTRAQ. *Agronomy* **2022**, *12*, 3207. <https://doi.org/10.3390/agronomy12123207>

Academic Editor: Debora Fontanini

Received: 2 November 2022

Accepted: 12 December 2022

Published: 16 December 2022

Publisher's Note: MDPI stays neutral with regard to jurisdictional claims in published maps and institutional affiliations.



Copyright: © 2022 by the authors. Licensee MDPI, Basel, Switzerland. This article is an open access article distributed under the terms and conditions of the Creative Commons Attribution (CC BY) license (<https://creativecommons.org/licenses/by/4.0/>).

1. Introduction

Rice (*Oryza sativa* L.) provides food for over 50% of the world's population, but world food production rates will increase by at least 50% by 2050 to meet the needs of a growing population [1]. Thus, further increasing rice production is essential to meet the future demand for food. Improvement of yield based solely on plant type and increased fertilizer application has been very difficult. A total of 90–95% of the organic matter in crop yield comes from photosynthetic products. The light energy utilization rate of existing high-yielding rice varieties is 1.0–1.5%, but the ideal value is about 3–5%. The

plant canopy structure cannot be changed, so efforts to improve rice yield have shifted from the selection of ideal plant types to improvement of the leaf photosynthetic rate [2]. Improving the photosynthesis and energy conversion efficiency is an important approach to promote crop yield [3–5]. High-light-efficiency germplasm resources can be used as material sources to investigate photosynthetic function. The photosynthetic productivity of crops mainly depends on light energy interception capacity and light energy conversion efficiency, with the former related to the development of leaf area and the latter related to the single-leaf photosynthetic rate. In addition to photosynthetic rate, photosynthetic functional period, chlorophyll content, and quantum efficiency are important parameters of photosynthetic function [6]. Additionally, C_3 plant photosynthesis can be significantly affected by leaf conductance and stomatal conductance, and the introduction of C_4 plant genes can increase the CO_2 concentration and the expression of ribulose-1,5-bisphosphate carboxylase (Rubisco) in rice leaves, thus increasing the overall leaf photosynthetic rate [7]. Studies on photosynthetic functions in rice have been limited to physiological level analysis and gene localization, with limited studies using proteomic techniques to identify key photosynthetic proteins.

Taking advantage of the geographical and natural environment of Guangxi, our team has established a large collection of rice germplasm resources in Southeast Asia and worked to evaluate the differences in the photosynthetic characteristics of these resources. We screened photosynthetic characteristics of ~220 Southeast Asian rice germplasm resources, and found the net photosynthetic rate (Pn) of a single leaf varied from $11.26 \mu\text{mol m}^{-2} \text{S}^{-1}$ for G164 to $36.96 \mu\text{mol m}^{-2} \text{S}^{-1}$ for C1—a three-fold difference—and the net photosynthetic rate of C1 is close to that of C_4 plant maize. However, the underlying mechanisms explaining this three-fold difference in the photosynthetic rate of C1 compared to G164 were not known. We hypothesized that significant differences in leaf tissue structure, chloroplast ultrastructure, photosynthetic key enzymes, and chlorophyll fluorescence parameters and protein might explain the difference between C1 and G164.

In this study, we systematically investigated the underlying mechanisms explaining the high Pn of C1 germplasm and the low Pn of G164 by analyzing the tissue structure, chloroplast ultrastructure, and photosynthetic physiological characteristics, and by applying proteomic methods. The results of our study improve our understanding of the physiological basis of the high photosynthetic rate of C1 germplasm and lay the foundation for analysis of related genes and practical breeding utilization.

2. Materials and Methods

2.1. Plant Material and Experimental Design

Two Southeast Asian rice germplasm varieties, C1 and G164, were used in this study. The experiment was conducted from plants cultivated in early planting in 2021 at the Rice Research Institute of Guangxi Academy of Agricultural Sciences Institute, China ($108^{\circ}14'51''$ E, $22^{\circ}50'54''$ N). The soil in the experimental field is clay (Ultisol, USDA taxonomy) with the following properties: pH = 6.10, organic matter = 20.6 g kg^{-1} , available N = 79 mg kg^{-1} , available P = 28 mg kg^{-1} , and available K = 71 mg kg^{-1} . Soil testing was performed using samples obtained from the upper 20 cm layer prior to planting in 2021. C1 and G164 were each planted in five rows of 16 plants each, with a planting area of $16 \text{ cm} \times 20 \text{ cm}$. Routine water, fertilizer, and pest and disease control practices were utilized. In the heading and flowering stage, sword leaves were taken to measure morphological indicators including leaf tissue structure and chloroplast ultrastructure; physiological indicators including photosynthetic characteristics, chlorophyll fluorescence parameters, chlorophyll content (soil and plant analyzer development, SPAD) and relative steady phase of chlorophyll content (RSP); and proteomics. Three biological replicates were performed for each indicator.

2.2. Investigations and Measurements

2.2.1. Leaf Tissue Structure

Ten small pieces with dimensions of 1 cm × 0.2 cm were cut from the middle of sword leaves of each variety, fixed with FAA fixative, and dehydrated with ethanol. The samples were paraffin embedded, sliced on a Leica RM2235 microtome (Leica Microsystems, Solms, Germany) at a thickness of 8 µm, and prepared as permanent sections with saffron-solid green counterstain (1% saffron and 0.5% solid green) and toluidine blue. Samples were subjected to microscopic examination, photography, and observation using Image-pro plus 6.0 (Media Cybernetics, Inc., Rockville, MD, USA) for analysis.

2.2.2. Chloroplast Ultrastructure

Ten sword leaves of each material were subjected to electron-microscope ultrastructure observation. The rapier leaves were interrupted at the heading and flowering stage, and 4–5 small strips with a width of 1 mm and length of 2–3 mm were cut with sharp scissors and immediately placed in pre-cooled 2.5% (pH 7.2) glutaraldehyde for pumping until they sank. After 2 h, the leaves were rinsed three times with 0.1 mmol L⁻¹ phosphate buffer (pH 7.4) for 15 min each time and then dehydrated with gradient-concentration acetone, impregnated with epoxy resin, and embedded. After polymerization into embedding blocks, the leaves were cut into 60–80 nm ultrathin sections on a Leica UC7 ultramicrotome (Leica Microsystems CMS GmbH, Wetzlar, Germany), sliced with a 150-mesh copper mesh, and double stained with uranyl acetate and citric acid. Finally, images were collected and analyzed under a HITACHI HT7800 transmission electron microscope (Hitachi High-Technologies Ltd., Narco, Japan).

2.3. Physiological Indicators

2.3.1. Photosynthetic Characteristics

Photosynthetic characteristics of Pn, stomatal conductance (Gs), intercellular CO₂ concentration (Ci), and transpiration rate (Tr), were measured using an LI-6400XT portable photosynthesis measurement system (Li-6400 XT, LI-COR Inc., Lincoln, NE, USA). The following method of measurement was used. During the heading and flowering stage, the light intensity was set at 1500 µmol m⁻² s⁻¹, the temperature was 28 °C, the CO₂ concentration was 380 µL L⁻¹, and gas flow rate was set to 500 µmol s⁻¹. The upper and middle leaf parts were selected for measurement, with three replicates per plant.

2.3.2. Chlorophyll Fluorescence Parameters

Three sword leaves with the same growth at the heading and flowering stages were selected, dark-adapted for 30 min, and measured using the LI-6400XT portable photosynthesis measurement system (Li-6400 XT, LI-COR Inc., Lincoln, NE, USA), with measurements performed three times. The minimal fluorescence (F₀), maximum fluorescence (F_m), minimal fluorescence in light (F₀'), maximal fluorescence in light (F_m'), fluorescence in the stable state (F_s), the maximum photochemical quantum yield of photosystem II (PSII) (F_v/F_m), and the photochemical burst (qP) were calculated from the measured values [8]. Photochemical quenching (qP), non-photochemical quenching (NPQ), electron transport rate (ETR), and the fraction of absorbed light energy used for pigment dissipation in the PSII antennae (%D) were determined, where $F_v/F_m = (F_m - F_0)/F_m$, $\Phi_{PSII} = (F_m' - F_s)/F_m'$, $qP = (F_m' - F_s)/(F_m' - F_0')$, and $NPQ = (F_m - F_m')/F_m'$.

2.3.3. Chlorophyll Content SPAD and RSP

Chlorophyll content was measured using a SPAD-502 Plus chlorophyll meter (Konica Minolta, INC., Tokyo, Japan). The middle of the leaf and the upper and lower leaf parts were about 3 cm away from the middle and were each measured once (avoiding the midvein of the leaf), and the average of three measurements was calculated as the SPAD measurement value of the leaf. RSP was measured during the period from the leaf sheath

of the sword leaf until the yellowing of the leaf, with chlorophyll content measured by SPAD-502 Plus chlorophyll analyzer.

2.3.4. Rubisco Enzyme Activity and Content

Rubisco enzyme activity and content were determined following the method of Li et al. [9].

2.4. *i*TRAQ Proteomics

2.4.1. Protein Extraction, Trypsin Digestion and *i*TRAQ Labeling

Samples were ground with liquid nitrogen and then the powder was transferred to a 5 mL centrifuge tube and sonicated three times on ice in lysis buffer using a high intensity ultrasonic processor (Scientz, Ningbo, China). An equal volume of tris-saturated phenol (pH 8.0) was added and mixed. After centrifugation (4 °C, 10 min, 12,000 × *g*), the upper phenol phase was transferred to a new centrifuge tube. At least four volumes of ammonium sulphate-saturated methanol were added to precipitate the protein and the mixture was incubated at −20 °C for at least 6 h. The remaining precipitate was washed with ice-cold methanol, followed by three washes of ice-cold acetone. The precipitated protein was redissolved in 8 M urea, and the protein concentration was determined using a BCA kit (A045-4-2, NanJing JianCheng Institute of Biological Engineering Ltd., Nanjing, China).

The protein solution was reduced with 5 mM dithiothreitol for 30 min at 56 °C, and then alkylated with 11 mM iodoacetamide for 15 min at room temperature in the dark. The protein sample was diluted into 100 mM triethylammonium bicarbonate (TEAB) urea at a concentration of less than 2 M. Finally, trypsin was added at a 1:50 trypsin-to-protein mass ratio for overnight digestion, followed by a second addition at a 1:100 trypsin-to-protein mass ratio and digested for 4 h.

After trypsin digestion, the peptide solution was desalted by Strata × C18 SPE column (Phenomenex) and vacuum-dried. The peptides were reconstituted in 0.5 M (TEAB) and processed according to the *i*TRAQ kit manufacturer's protocol. Briefly, one unit of *i*TRAQ reagent was thawed and reconstituted in acetonitrile. The peptide mixtures were then incubated at room temperature for 2 h, pooled, desalted, and dried by vacuum centrifugation.

2.4.2. High-Performance Liquid Chromatography (HPLC) Fractionation

High-pH reverse-phase HPLC was utilized to separate the tryptic peptides using an Agilent 300 Extend C18 column (5 μm particles, 4.6 mm ID; 250 mm length). The peptides were initially divided into 60 sections over the course of 60 min using a gradient of 8% to 32% acetonitrile (pH 9.0). Then, the peptides were divided into 18 sections and vacuum centrifuged dried.

2.4.3. Liquid Chromatography (LC) Tandem Mass Spectrometry (MS/MS) Analysis

The tryptic peptides were dispersed in 0.1% formic acid (solvent A) before being immediately put onto a home-made reversed-phase analytical column (15 cm length, 75 μm i.d.). An EASY-nLC 1000 ultra-performance LC (UPLC) system was used to complete the gradient, which involved increasing solvent B from 6% to 23% (0.1% formic acid in 98% acetonitrile) over the course of 26 min, from 23% to 35% in 8 min, to 80% in 3 min, and then holding it at 80% for the final 3 min. The peptides were subjected to NSI source followed by MS/MS in Q Exactive™ Plus (Thermo Fisher Scientific Inc., Bremen, Germany) coupled online to UPLC. The electrospray voltage applied was 2.0 kV. Intact peptides were found in the Orbitrap with a resolution of 70,000 in the *m/z* scan range of 350 to 1800. The fragments were detected in the Orbitrap at a resolution of 17,500 after peptides were then selected for MS/MS using the NCE setting at 28. A data-dependent procedure alternated between one MS scan followed by 20 MS/MS scans with 15.0 s dynamic exclusion. Automatic gain control was set at 5×10^4 and a fixed first mass was set as 100 *m/z*.

2.4.4. Database Search

The search engine MaxQuant was used to process the generated MS/MS data (v.1.6.15.0). Tandem mass spectra were compared with the 20,422 entries SwissProt database concatenated with reverse decoy database. The cleavage enzyme, trypsin/P, was designated and permitted up to two missed cleavages. The mass tolerance for precursor ions was set as 20 ppm in first search and 5 ppm in the initial search, and the mass tolerance for fragment ions was set as 0.02 Da.

2.5. Bioinformatics Analysis

2.5.1. Gene Ontology (GO) Annotation

Proteomic data were obtained from the UniProt-GOA database (<http://www.ebi.ac.uk/GOA/>, accessed on 14 September 2021). First, each identified protein ID was converted to UniProt ID and then mapped to GO IDs. If several identified proteins were not annotated by the UniProt-GOA database, InterProScan software was used to annotate the protein's GO functional property based on protein-sequence alignment. Then, the proteins were classified by GO annotation into three categories: biological process, cellular component, and molecular function.

2.5.2. Domain Annotation

The identified protein domains and functional descriptions were annotated using InterProScan (a sequence analysis application) based on protein sequence alignment and using the InterPro domain database (<http://www.ebi.ac.uk/interpro/>, accessed on 14 September 2021). This database integrates diverse information about protein families, domains, and functional sites central to the database are diagnostic models, known as signatures, against which protein sequences can be searched to determine their potential function. InterPro can be used for the large-scale analysis of whole and meta-genomes and characterization of individual proteins.

2.5.3. Sequence Subcellular Localization

We used WoLF PSORT, a subcellular localization prediction software (v.1.0 <https://wolfsort.hgc.jp/>, accessed on 14 September 2021), to predict subcellular localization.

2.5.4. Enrichment of GO Analysis

Proteins were classified by GO annotation into three categories: biological process, cellular compartment, and molecular function. For each category, a two-tailed Fisher's exact test was employed to test the enrichment of differentially expressed proteins against all identified proteins. GO values with a corrected p -value < 0.05 were considered significant.

2.5.5. Enriched Pathway Analysis

The Kyoto Encyclopedia of Genes and Genomes (KEGG) database was used to identify enriched pathways by a two-tailed Fisher's exact test to assess the enrichment of differentially expressed proteins against all identified proteins. A pathway with a corrected p -value < 0.05 was considered significant. These pathways were classified into hierarchical categories as described on the KEGG website.

2.6. Real-Time Quantitative PCR Analysis

RNA was extracted with a kit (RA106-02, Biomed Genetic Technology Co., Beijing, China) and measured by real-time quantitative PCR (qRT-PCR) assay. The GAPDH gene was used as the reference control in the study. All qRT-PCR reactions were performed using a CFX96 system (Bio-Rad laboratories, Inc., Singapore).

2.7. Statistics and Analysis

The experimental data were analyzed and processed using Microsoft Office Excel 2010, and SPSS 19.0 was used for significance analysis. Analysis of variance (ANOVA) was

performed using the least significant difference LSD test, which at the 0.01 and 0.05 level were used to determine the difference between the means of each treatment. In proteomics, the fold change value of differential proteins was tested by *t*-test.

3. Results

3.1. Differences in Leaf Structure

Table 1 shows that compared to G164, C1 had higher stomatal density, stomatal size, LT, and numbers of big vascular bundles (BCBs) and small vascular bundles (SCBs), whereas the areas of BCB and SCB, vessel (V) diameter, and size of mesophyll cells were higher in G164 than C1 (Figure 1). C₃ plants perform photosynthesis in mesophyll cells, and vascular bundle cells transport metabolic-related products to leaf veins and provide structural support for leaves [10]. The results show that photosynthetic rate is more closely related to the numbers of BCB and SCB, and the stomatal characteristics.

Table 1. Differences in leaf tissue structure of rice germplasm resources of different photosynthetic efficiencies.

Name	Stomatal Density (pcs)	Stomatal Size (mm)	LT (mm)	No. of BCB (pcs)	No. of SCB (pcs)	BCB Area (mm ²)	SCB Area (mm ²)	V Diameter (mm)	MC Size (mm ²)
G164	3.667 a	0.001 a	0.100 a	9 a	46 a	0.016 a	0.0029 a	0.0435 a	2.4×10^{-5} b
C1	6.000 b	0.004 b	0.098 a	20 b	61 b	0.015 a	0.0028 a	0.0345 b	1.9×10^{-5} a

Note: Data are means of three replicates. Different letters in rows represent significant ($p < 0.05$) differences between rice germplasm resources.

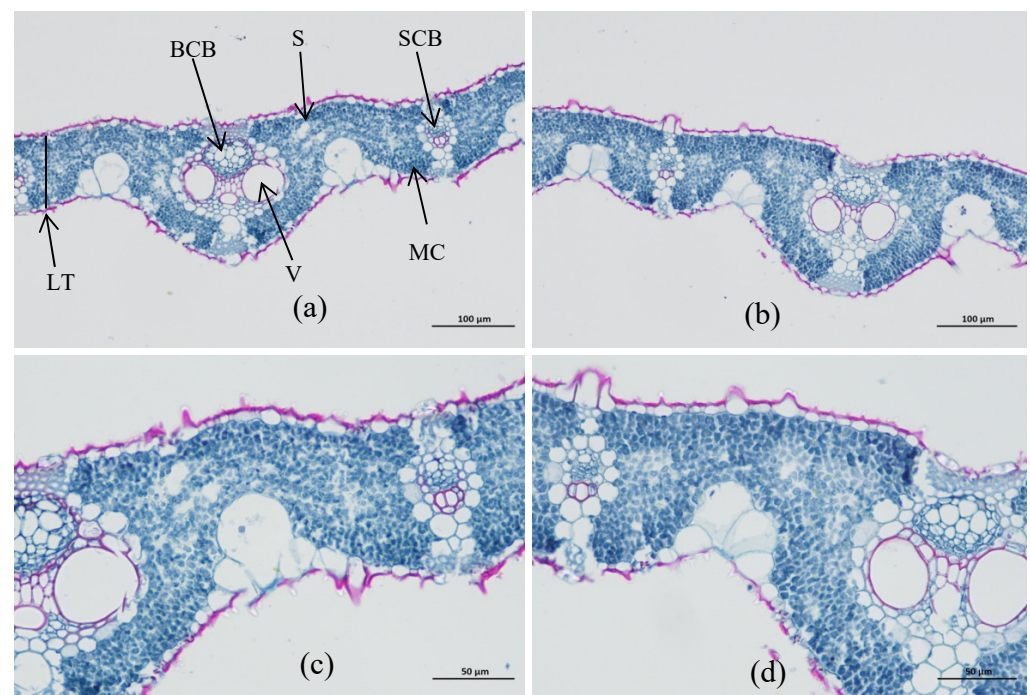


Figure 1. Leaf tissue structure of C1 and G164 rice germplasm resources. Note: (a,c) represent C1; (b,d) represent G164; BCB: big vascular bundle; SCB: small vascular bundle; LT: leaf thickness; V: vessel; MC: mesophyll cell; S: stomata.

3.2. Differences in Chloroplast Ultrastructure

The chloroplasts (Ch) of C1 sword leaves were neatly arranged in a spindle shape in the mesophyll cells. The thylakoid (Th) structure was complete, orderly, and densely arranged, and the lamellae were thick and compact along the long axis of the Ch. In contrast, the envelope and stroma in G164 Ch were separated, the edges were irregular,

and their lamellae were irregularly arranged (Figure 2). The vesicle-like lamellae were not uniformly arranged, the lamellae were thinner than those in C1, and the light-catching ability was relatively weak.

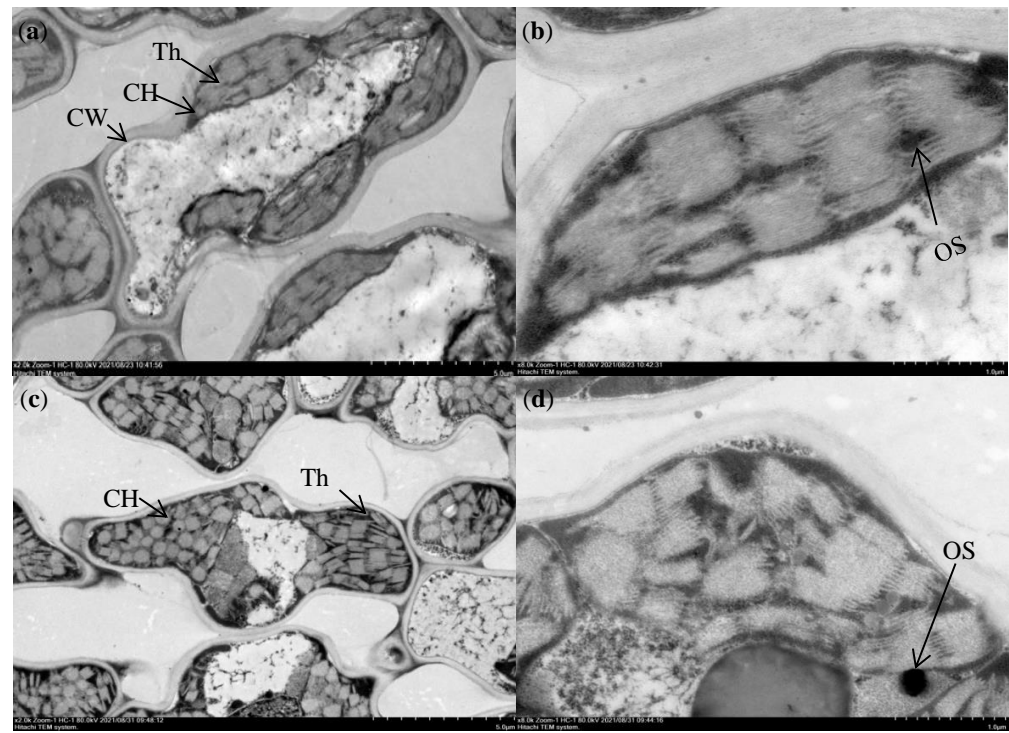


Figure 2. Chloroplast ultrastructure of leaves of C1 and G164 rice varieties. Note: (a,b) represent C1; (c,d) represent G164; Ch: chloroplast; CW: cell wall; Th: thylakoid; OS: osmiophilic granule.

3.3. Differences in Chlorophyll Value and Photosynthetic Rate

The difference in the photosynthetic efficiency (P_n) values between C1 and G164 was 3.26-fold, a significant difference. The RSP and SPAD values of C1 were 35.2% and 21.2% higher than those of G164, respectively. The RSP values were highly significantly different and the SPAD values were not significantly different between the two varieties (Figure 3).

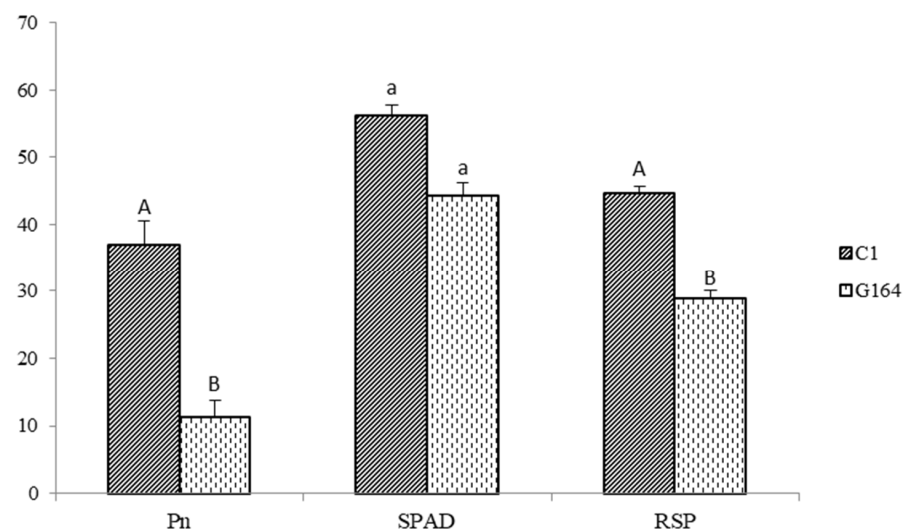


Figure 3. Photosynthetic rate and chlorophyll value of high- and low-light efficiency germplasm resources. Note: Data are means of three replicates. The uppercase and lowercase letters represent 1% and 5% level of significance of difference, respectively.

3.4. Differences in Chlorophyll Fluorescence Parameters and Rubisco

Chlorophyll fluorescence parameters of Fv/Fm, qP, ETR, and Φ PSII, were higher in C1 than in G164, and NPQ was higher in G164 than in C1, but these differences were not significant. In the heading and flowering stage, the activity and content of the key photosynthetic enzyme Rubisco in the sword leaves were higher in C1 than G164, with a significant difference in Rubisco activity between the two varieties (Table 2).

Table 2. Chlorophyll fluorescence parameters and enzyme characteristic of Rubisco in the sword leaves of high- and low-light efficiency germplasm resources C1 and G164.

Varieties	Fv/Fm	qP	NPQ	ETR	Φ PSII	Rubisco Activity (nmol/s/g)	Rubisco Content (ng/L)
C1	0.813 ± 0.006 a	0.911 ± 0.011 a	0.160 ± 0.055 a	30.429 ± 0.432 a	0.691 ± 0.009 a	5.311 ± 9.74 b	148.933 ± 2.95 a
G164	0.806 ± 0.002 a	0.874 ± 0.023 a	0.177 ± 0.042 a	28.954 ± 0.887 a	0.660 ± 0.019 a	5.037 ± 2.43 a	138.073 ± 4.28 a

Note: Data are means of three replicates. Different letters in rows represent significant ($p < 0.05$) differences between rice germplasm resources.

3.5. Proteomic Analysis of Different Germplasm Resources

3.5.1. Protein Identification and GO Analysis

The rice varieties C1 and G164 were next subjected to proteomic analysis by iTRAQ technology. Using 1.2-fold as the change threshold and a t-test p -value < 0.05 , three groups of repeats were compared. A total of 204 proteins showed up-regulated expression and 102 showed down-regulated expression in G164 compared to C1. Based on the GO annotation, the identified proteins were classified into three large categories of biological processes, cellular components, and molecular functions (45.5%, 28.3%, and 26.2%), and 30 small groups (Figure 4). The top three categories in each functional group were as follows: metabolic, molecular, and single biological processes in the biological process category; catalytic activity, binding, and antioxidant activity in the molecular function category; cells, organelles, and cell membranes in the cellular component category. The groups include 27 proteins related to photosynthetic operation: compared with G1, there are nine up-regulated proteins and 18 down-regulated proteins in G6 (Table 3).

Photosynthesis occurs in the chloroplasts, and the analysis revealed that most of the differential proteins are distributed in chloroplasts. Other differentially expressed proteins are found in the cytoplasm, nucleus, and mitochondria (Table 3). Compared with C1, G164 had ten differential proteins associated with photosynthetic electron transport in the photosynthetic pathway, with nine down-regulated proteins and one up-regulated protein. The down-regulated differential proteins included one ferredoxin (Fd) and three ferredoxin-NADP⁺ reductases (FNR), which are present on the vesicle-like surface; three PS II compound proteins (PSB28, PSB27, PSBP); two cytochrome b6-f complex iron-sulfur subunits (cytb6); and one plastocyanin (PC). Compared with C1, a total of 17 differential proteins were associated with CO₂ fixation in G164. Among these differential proteins, nine were up-regulated: two phosphoenolpyruvate carboxylases (PPC), one alanine transaminase (GPT), three malate dehydrogenases (MDH), one fructose-1,6-bisphosphatase I (FBP), one phosphoglycerate kinase (PGK), and one glyceraldehyde 3-phosphate dehydrogenase (GAPDH). There were eight down-regulated differential proteins: one triosephosphate isomerase (TPI), two glutamate-glyoxylate aminotransferases (GGAT), two malate dehydrogenases (MDH), phosphoglycerate kinase (PGK), two glyceraldehyde-3-phosphate dehydrogenase (NADP⁺) (GAPA), and ribulose-bisphosphate carboxylase small chain (Ru-BisCO, rbcS). Interestingly, the proteomics revealed that the C₄ key enzyme PEPC exhibited a higher content in G164 than in C1.

Table 3. Differential proteins associated with photosynthesis.

KEGG Pathway	Protein Accession	Protein Description	Coverage [%]	Fold Change	Direction of Change	Subcellular Localization
Photosynthesis	O23877	petH; ferredoxin—NADP ⁺ reductase [EC:1.18.1.2]	10.1	1.645 **	up	chloroplast
	P0C389	petA; apocytochrome f	46.2	0.764 **	down	nucleus
	P12123	petB; cytochrome b6	16.3	0.690 *	down	cytoplasm
	Q0DFC9	petE; plastocyanin	20.8	0.810 **	down	chloroplast
	Q0J8M2	petF; ferredoxin	40.3	0.790 **	down	chloroplast
	Q0JG75	psb28; PSII 13kDa protein	16.1	0.710 **	down	chloroplast
	Q109L0	psbP; photosystem II oxygen-evolving enhancer protein 2	17.7	0.645 **	down	chloroplast
	Q10LV7	psb27; photosystem II Psb27 protein	34.5	0.745 **	down	chloroplast
	Q69S39	petC; cytochrome b6-f complex iron-sulfur subunit [EC:1.10.9.1]	49.8	0.720 **	down	chloroplast
	Q6ZFJ3	petH; ferredoxin—NADP ⁺ reductase [EC:1.18.1.2]	56.3	0.770 **	down	chloroplast
Carbon fixation in photosynthetic organism	A0A0P0WP33	PGK; phosphoglycerate kinase [EC:2.7.2.3]	63.6	0.800 **	down	chloroplast
	A0A0P0XLG164	PEPC; phosphoenolpyruvate carboxylase [EC:4.1.1.31]	20.3	1.635 *	up	cytoplasm
	A0A0P0XUE4	GPT; alanine transaminase [EC:2.6.1.2]	22.4	1.425 *	up	cytoplasm
	Q0JJQ7	E1.1.1.40; malate dehydrogenase (oxaloacetate-decarboxylating) (NADP ⁺) [EC:1.1.1.40]	29.1	1.500 **	up	chloroplast
	Q2QTJ1	rbcS; ribulose-bisphosphate carboxylase small chain [EC:4.1.1.39]	53.1	0.790 **	down	chloroplast
	Q42972	MDH2; malate dehydrogenase [EC:1.1.1.37]	15.7	1.465 **	up	cytoplasm
	Q655Y9	FBP; fructose-1,6-bisphosphatase I [EC:3.1.3.11]	27.7	1.315 **	up	chloroplast
	Q69K00	TPI; triosephosphate isomerase (TIM) [EC:5.3.1.1]	53	0.745 **	down	chloroplast
	Q69UU3	GGAT; glutamate-glyoxylate aminotransferase [EC:2.6.1.4 2.6.1.2 2.6.1.44]	58.4	0.815 **	down	peroxisome
	Q6H6C7	PGK; phosphoglycerate kinase [EC:2.7.2.3]	55.7	1.300 **	up	chloroplast
	Q6YYW3	E1.1.1.82; malate dehydrogenase (NADP ⁺) [EC:1.1.1.82]	47.8	0.795 **	down	chloroplast
	Q7X8A1	GAPA; glyceraldehyde-3-phosphate dehydrogenase (NADP ⁺) (phosphorylating) [EC:1.2.1.13]	51	0.775 **	down	chloroplast
	Q7XDC8	MDH1; malate dehydrogenase [EC:1.1.1.37]	31.6	1.225 **	up	cytoplasm
	Q7XZW5	MDH2; malate dehydrogenase [EC:1.1.1.37]	57.9	0.750 **	down	chloroplast
	Q8H4V1	pepc; phosphoenolpyruvate carboxylase [EC:4.1.1.31]	35.7	1.310 **	up	cytoplasm
	Q9SNK3	GAPA; glyceraldehyde-3-phosphate dehydrogenase (NADP ⁺) (phosphorylating) [EC:1.2.1.13]	55	0.815 **	down	chloroplast
	Q0J8A4	GAPDH; glyceraldehyde 3-phosphate dehydrogenase [EC:1.2.1.12]	64.1	1.390 **	up	cytoplasm

Note: Data are means of three replicates. ** and * represent 1% and 5% level of significance of difference respectively.

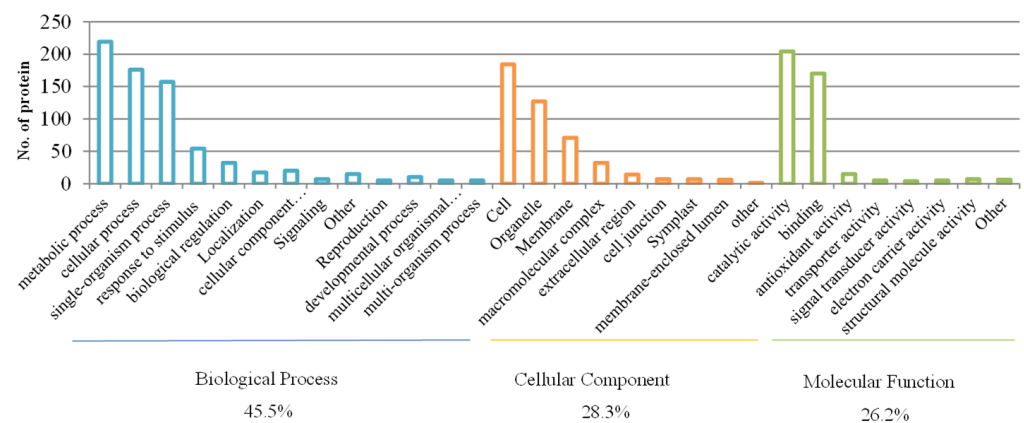


Figure 4. Distribution of differentially expressed proteins by second-level GO annotation.

3.5.2. Classification of Subcellular Structure Localization

Subcellular structure prediction and classification were performed for differentially expressed proteins using WoLF PSORT software V1.0 (Figure 5). A total of 89 and 77 of the up-regulated and down-regulated proteins, respectively, were distributed in the chloroplasts in G164 compared to C1 (Figure 5a). The chloroplasts are the most widely distributed of the subcellular structures (Figure 5b).

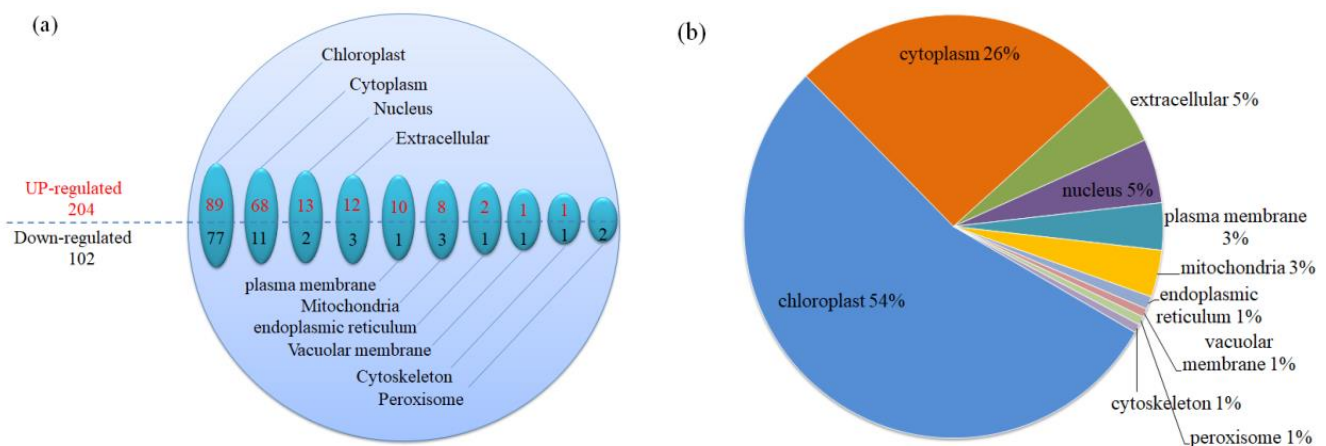
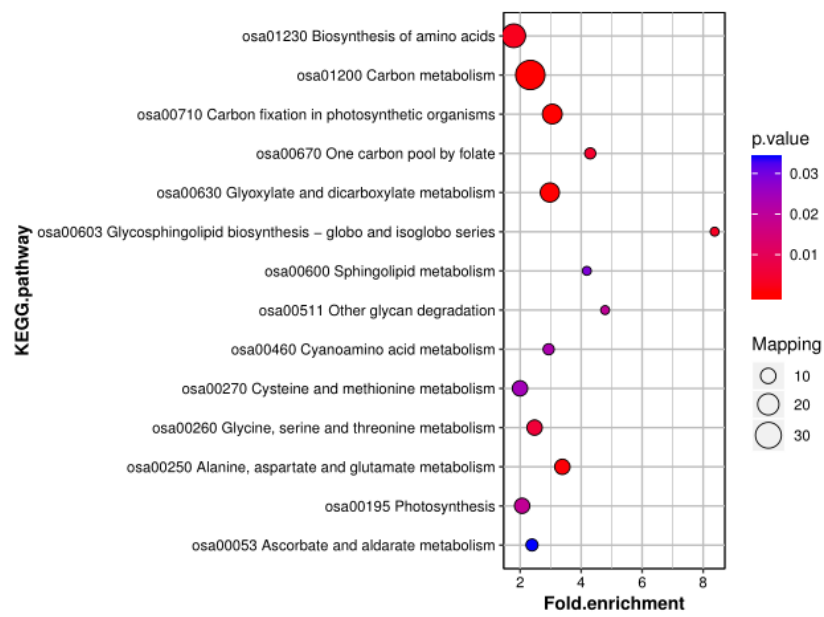


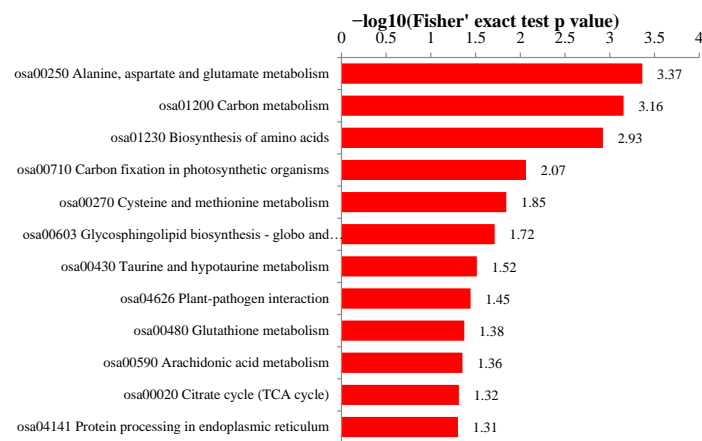
Figure 5. Subcellular structure localization and distribution of up-regulated and down-regulated proteins in G164 compared to C1. Note: Location and number of up-regulated and down-regulated proteins in the subcellular (a), and Location and ratio of differential proteins in the subcellular (b).

3.5.3. KEGG Analysis

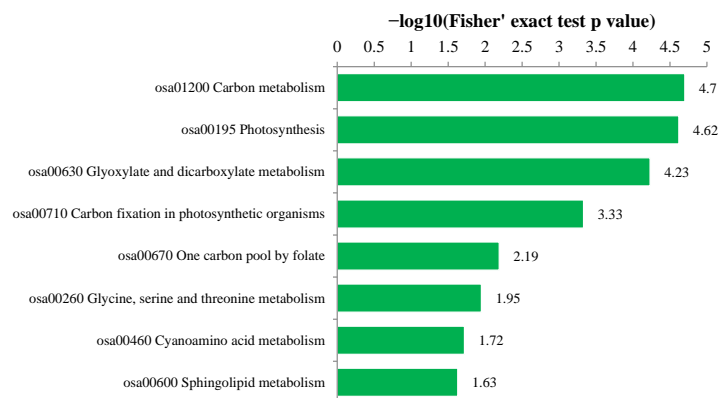
The KEGG information network includes known molecular interactions, such as metabolic pathways, complexes, and biochemical reactions. Based on KEGG pathway differential protein enrichment (Figure 6a), the most enriched protein metabolic pathway is carbon metabolism (osa01200), the second highest enriched metabolic pathway is the biosynthesis of amino acids (osa01230), followed by carbon fixation in photosynthetic organisms pathway (osa0710), and the glyoxylate and dicarboxylate metabolism pathway (osa00630), with thirty-eight, twenty-five, seventeen, and fourteen enriched proteins, respectively; all were enriched at a very significant level. The photosynthesis pathway (osa00195) was also significantly different, with eleven enriched proteins. The metabolic pathways associated with photosynthesis are carbon fixation in photosynthetic organisms (osa01200) and photosynthesis (osa00195). KEGG pathways of up-regulated and down-regulated proteins related to photosynthesis are shown in Figure 6b,c, respectively. Values on the horizontal axis are negative log-transformations of significant p -values ($p < 0.05$).



(a)



(b)



(c)

Figure 6. KEGG pathway enrichment of photosynthetic enzymes; all proteins (a), up-regulated proteins (b), and down-regulated proteins (c). Note: Values on the horizontal axis are negative log-transformations of significant p -values ($p < 0.05$).

Differentially expressed genes and proteins were mapped to the “Photosynthesis” and “Carbon Fixation In Photosynthetic Organism” KEGG Pathways. In these pathways, nine genes involved in photosynthesis in rice leaves were selected for real-time PCR validation to determine if gene expression data would confirm the changes in protein abundance. The expression levels of these six genes (Os07g0147900, Os09g0315700, Os10g0390500, P0585H11.115, PetE, and Os05g0496200) were consistent with the proteomic data (Figure 7 and Table 3). Compared to C1, Os07g014790 (petH), Os09g0315700 (ppc), and Os10g0390500 (GPT) were more highly expressed in G164, and P0585H11.115 (GGAT), PetE, and Os05g0496200 (PGK), were expressed at a lower level in G164.

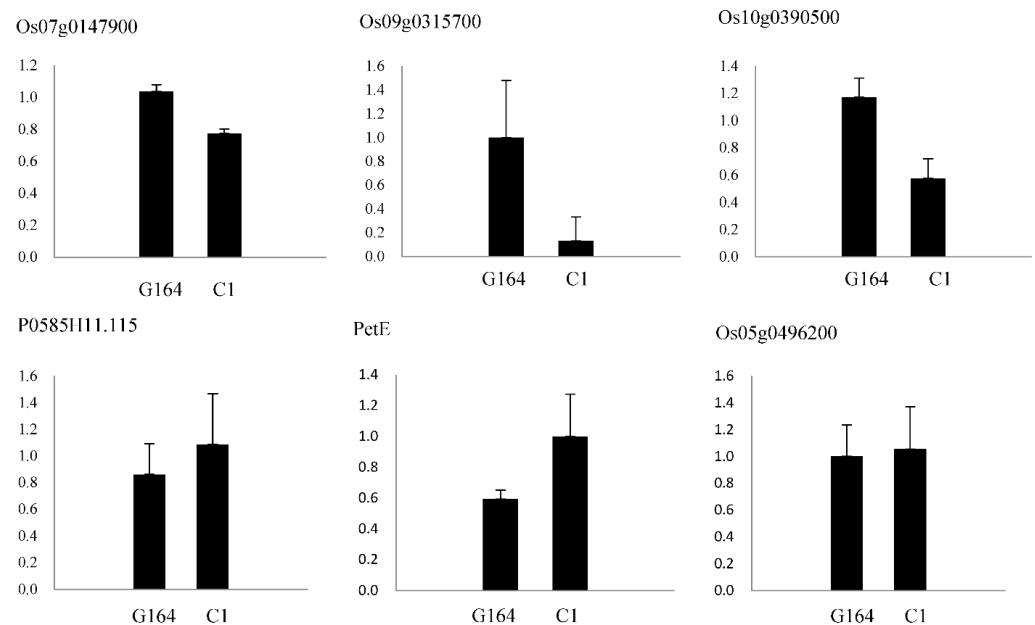


Figure 7. Expression analysis of nine genes in leaves of C1 and G164 using real-time PCR. Note: Os07g0147900: ferredoxin—NADP⁺ reductase (petH); Os09g0315700: phosphoenolpyruvate carboxylase (ppc); Os10g0390500: alanine transaminase (GPT); P0585H11.115: glutamate-glyoxylate aminotransferase (GGAT); PetE: plastocyanin (petE); Os05g0496200: phosphoglycerate kinase (PGK).

4. Discussion

As a C₃ plant, the regulation of photosynthesis in rice involves a complex metabolic network involving stages of light and dark reactions. Photosynthesis occurs in the chloroplasts, an organelle specific to plant cells, and the light reactions of photosynthesis occur in the thylakoid membranes of the chloroplasts. The light reactions of photosynthesis include the absorption and conversion of light energy, water decomposition, electron transfer, reduction of NADP, formation of a proton gradient across the thylakoid membrane, and synthesis of ATP. The dark reaction, or Calvin cycle, occurs in the Ch stroma of the chloroplast cells, and mainly includes the assimilatory force of NADPH and CO₂ carboxylation -. The improvement of photosynthesis requires the coordination of these two stages of physiological metabolism for balance of light energy absorption and utilization. Various strategies have been used to improve the photosynthetic capacity in crops, such as increasing the activity of Calvin cycle enzymes to increase the rate of carboxylation [11], increasing the rate of photosynthetic electron transfer across the Th membrane [12], modifying leaf anatomy to improve light energy capture rate and leaf pulp conductance [13], and introduce C₄ photosynthetic pathway into C₃ crops [14]. More than 80% of rice grain yield comes from the three functional leaves, of which the sword leaf contributes the greatest yield. Therefore, the sword leaves were selected for detailed analysis in this study.

4.1. Effect of Tissue Structure on Pn

The leaf structure provides the structural framework for photosynthesis and gas exchange [15]. Pn is significantly positively correlated with Gs and mesophyll conductance (Gm) [16], which is one of the largest limiting factors of Pn [17,18]. Gs is mainly influenced by stomatal size, density, distribution, and opening, and the higher the stomatal density, the lower the stomatal transmission resistance and the more favorable the improvement of light energy, CO₂ utilization efficiency, and gas exchange capacity, thus increasing Pn and potential photosynthetic capacity [19]. In this study, the stomatal density, stomatal size, and the number of vascular bundles of C1 were significantly higher than those of G164, showing that under the same natural conditions, except Gs and Gm, vascular bundle size is not only responsible for the translocation of metabolites into leaf veins and providing structural support, but also had a significant effect on photosynthetic function. This is consistent with the findings of Huang and coworkers [20] suggesting the manipulation of vascular bundles can improve photosynthesis in rice plants. In this study, compared to C1, leaf thickness was greater in G164, though this difference was not significant. As an important leaf structural trait determining leaf photosynthesis, leaf thickness has usually been found to be positively related to Pn [21,22].

Photosynthesis occurs mainly in the chloroplasts of mesophyll cells, as observed from the chloroplast ultrastructure. C1 Mesophyll cells have more chloroplasts, regular thylakoid structure, and complete and orderly arranged lamellae. The high number of cystoid layers increases the contact area with light and enhances the light absorption of chloroplasts function transfer and transformation, which promote the formation and accumulation of photosynthetic products [23]. The neat and tight lamellae shorten the electron transfer distance and improve the ability to capture and absorb light energy and photosynthetic electron transfer rate. This may be an important structural basis for high light efficiency mechanism.

4.2. Effect of Photosynthetic Physiological Indicators on Pn

Photosynthesis in C₃ plants can be affected by the activity of Rubisco, ribulose-1,5-bisphosphate (RuBP) regeneration, and release of phosphate during the metabolism of triose phosphate to either starch or sucrose [24]. Rubisco is a key enzyme in determining the photosynthetic capacity of C₃ plants. The results of this study showed higher content and activity of Rubisco in C1 than in G164, with enzyme activity significantly different between the two varieties. The photosynthetic capacity of the upper leaves of super hybrid rice showed that Rubisco enzyme activity rather than C determines the photosynthetic capacity of rice leaves. Rubisco content was positively correlated with the photosynthetic rate during plant growth and senescence, and the Rubisco activity of the high yield potential rice variety was significantly higher than that of common varieties. Thus, the Rubisco enzyme activity increased with the increase in stomatal density, with a significant correlation between the two, indicating that increasing stomatal density can promote the activity of Rubisco to improve the potential photosynthetic capacity of rice. This is consistent with greater stomatal density and Rubisco enzyme activity in C1 compared to G164.

Chlorophyll fluorescence parameters not only reflect the absorption, transfer, and dissipation allocation of light by the plant leaf PS but also relate to CO₂ fixation, electron transfer, and proton gradient establishment [25]. Fv/Fm reflects the maximum efficiency of using absorbed light energy for chemical reactions in PSII reactions, and can vary depending on pigmentation, cell structure, temperature and light conditions, and nutrient status. The qP value reflects the proportion of PSII pigment absorption for photochemical electron transfer and the level of photosynthetic activity; ΦPSII is often used to reflect electron transfer between PSII and PSI, with the larger the value, the faster the electron transfer efficiency [26]. NPQ reflects the portion of light energy absorbed by PSII antenna pigments that cannot be used for photosynthetic electron transfer so is dissipated in the form of heat; the smaller its value, the smaller the heat dissipation and the more favorable the yield accumulation. The electron transport rate (ETR) value can be used as an important indicator

of photosynthesis and reflects the electron transfer efficiency under light conditions. ETR is related to limited RuBP regeneration. In this experiment, Fv/Fm, qP, ETR, and Φ PSII of C1 were higher than those of G164, and NPQ was higher in G164 than in C1, suggesting the physiological basis for the higher light absorption, higher transfer efficiency, fast conversion rate, and photosynthetic efficiency of C1 compared to G164.

4.3. Differential Proteins among High- and Low-Light-Efficiency Germplasm Resources

Identification of the proteins that play crucial roles in photosynthesis and carbon assimilation is required to develop plants with improved photosynthetic performance and enhanced nutritional value [27]. In this study, 27 photosynthesis-related differential proteins were identified by iTRAQ proteomic analysis of sword leaves at the heading and flowering stages (Table 3). Of the 27 proteins, 10 and 17 of the identified proteins are related to photosynthetic electron transport and carbon assimilation, respectively. Electron transport-related proteins include Fd, FNR, cytb6/f, PC, and oxygen release compound proteins (Psb27, Psb28, and PsbP). Under iron deficiency, PSI core, Cytb6/f, and Rubisco were most diminished, followed by OEC and LHCII, thereby further affecting the photosynthetic function of chloroplasts [28]. The down-regulated proteins are essential components of PSI, NDH, and the Cytb6f complex under spaceflight microgravity environmental stresses [29], indicating that photosynthetic function is hindered by compromised electron transport. In the oxygen emission center (OEC), Psb27 is involved in the photorecovery of PSII and promotes the assembly of manganese clusters to PSII. Psb28 is an exogenous protein of PSII that accelerates the photodamage repair of PSII under high temperature and intense light [30]. PsbP (23 kDa) is one of the three subunits of the PSII OEC and affects the assembly and stability of PSII. Enhanced abundance of the ferredoxin NADPH reductase, the 23 kDa polypeptide of photosystem II, and a FtsH-like protein therefore reflect an approach to attenuate aggravating effects of Na1 on the photosynthetic machinery [31]. This study showed that proteins in the electron transport chain determine the electron transport of PSII to PSI, for improved light-efficiency in germplasm C1. Fan et al. [32] found increased light capture efficiency of PSII but decreased capacity from PSII transmitted to PSI in soybean leaves under shade condition, causing decreased photosynthetic capacity in shading [33]. Overall, the photosynthetic differences in rice germplasm resources mainly depend on light-responsive electron transfer and carbon assimilation in leaves rather than on the light-capture pathway; this result is consistent with that of a previous study by Feng [34].

An important regulatory mechanism of photosynthesis is the control of enzyme levels. Several differential proteins identified in this study act in the CO₂ fixation pathway. This study found differences in the levels of enzymes and proteins in the two germplasm resources. The down-regulated differential proteins included phosphoglycerate kinase (PGK), triose phosphate isomerase (TPI), glutamate-glyoxylate aminotransferase (GGAT), glyceraldehyde-3-phosphate dehydrogenase (GAPDH), and ribulose-bisphosphate carboxylase small chain (rbcS). These enzymes play a central role in the Calvin cycle, including catalysis, conversion, and carboxylation, and the down-regulation of these proteins resulted in impaired carbon assimilation and reduced photosynthetic efficiency. Interestingly, GGAT is a photorespiration enzyme and when down-regulated, preferentially catalyzes the conversion of glyoxylate to glycine [35]. When leaf stomata are closed or external CO₂ concentration is low, the GGAT catalytic rate decreases, affecting carbon recovery in the C₃ pathway and indirectly affecting CO₂ assimilation.

Among the differential proteins related to carbon fixation, MDHs in chloroplasts (pMDH) were all down-regulated and cytoplasmic MDHs (cMDH) were all up-regulated. The differentially located MDHs have different functions. During carbon fixation, cMDH is involved in pyruvate metabolism, oxidizing malate in the mitochondrial matrix to oxaloacetate and then converting it to sucrose through the sugar xenobiotic pathway to accumulate starch, and pMDH is important for fixing CO₂ and increasing photosynthetic yield.

In addition to Rubisco (rbc_s), sedoheptulose-1,7-bisphosphatase (SBPase) and fructose-1,6-bisphosphatase (FBPase) were identified by the traditional kinetic parameter method as key enzymes of the Calvin cycle. PGK, TPI, GGAT, GAPDH, and cMDH also play crucial roles in these reactions.

Interestingly, C₄ cycle key enzyme phosphoenolpyruvate carboxylase (PEPC) showed a higher level in G164 than in C1. Some experts have reported that the distinction between C₃ and C₄ plants may not be absolute, and suggested the possible presence of the C₄ pathway in C₃ plants [36]. Agarie et al. [37] and Fukayama et al. [38] reported that PEPC overexpression actually decreased the final net photosynthetic rate due to the increase in dark respiration rate. Ku et al. [39] transferred *pepc* and *ppdk* from maize into rice and found that the photosynthetic capacity of transgenic rice increased by 35%, due to an increase in stomatal CO₂ transfer capacity and an increase in internal CO₂ concentration. This may explain why the photosynthetic rate was not higher in G164 than in C1.

5. Conclusions

The results indicated that compared with the high P_n germplasm resource C1, the decrease in photosynthesis in the low-light-efficiency germplasm resource G164 is associated with the regulation of leaf structure, Ch ultrastructure, and the levels of proteins related to photosynthesis and the carbon cycle. These results suggest that (1) vascular bundle characteristics, stomata, and Th characteristics have a great influence on the photosynthetic rate; (2) most of the proteins involved in electron transfer from PS II to PSI and several proteins (PGK, TPI, GGAT, cMDH, and GADPH) related to carbon fixation in photosynthetic organisms are closely related to the photosynthetic rate, and increasing the levels of such proteins can effectively enhance P_n; (3) C1 can be used as a donor material for selection of high light efficiency varieties and in-depth photosynthesis studies.

Author Contributions: Conceptualization, T.L.; software, H.W. and R.L.; investigation, X.Z., M.T., Q.W. and L.C.; data curation, W.T. and L.C.; writing—original draft preparation, X.Z. and T.L.; writing—review and editing, H.W. and G.G.; funding acquisition, T.L., M.T. and X.Z. All authors have read and agreed to the published version of the manuscript.

Funding: This research was funded by Program on the Natural Science Foundation of Guangxi Province, grant number 2021GXNSFAA220026 and 2021GXNSFAA220093, National Modern Agricultural Technology System Guangxi Innovation Team, nycytxgxcxd-2021-01-04, the Advantage Team Project of Guangxi Academy of Agricultural Sciences, 2021YT031, and The Open Fund of the Guangxi Key Laboratory of Rice Genetics and Breeding, 2022-36-Z01-KF09.

Data Availability Statement: The data presented in this study are available on request from the corresponding author.

Conflicts of Interest: The authors declare no conflict of interest.

References

1. Murchie, E.H.; Pinto, M.; Horton, P. Agriculture and the new challenges for photosynthesis research. *New Phytol.* **2009**, *181*, 532–552. [[CrossRef](#)] [[PubMed](#)]
2. Horton, P. Prospects for crop improvement through the genetic manipulation of photosynthesis: Morphological and biochemical aspects of light capture. *J. Exp. Bot.* **2000**, *51*, 475–485. [[CrossRef](#)] [[PubMed](#)]
3. Long, S.P.; Marshall-Colon, A.; Zhu, X.-G. Meeting the Global Food Demand of the Future by Engineering Crop Photosynthesis and Yield Potential. *Cell* **2015**, *161*, 56–66. [[CrossRef](#)] [[PubMed](#)]
4. Adachi, S.; Yamamoto, T.; Nakae, T.; Yamashita, M.; Uchida, M.; Karimata, R.; Ichihara, N.; Soda, K.; Ochiai, T.; Ao, R.; et al. Genetic architecture of leaf photosynthesis in rice revealed by different types of reciprocal mapping populations. *J. Exp. Bot.* **2019**, *70*, 5131–5144. [[CrossRef](#)] [[PubMed](#)]
5. Ye, M.; Peng, S.; Li, Y. Intraspecific variation in photosynthetic nitrogen-use efficiency is positively related to photosynthetic rate in rice (*Oryza sativa* L.) plants. *Photosynthetica* **2019**, *57*, 311–319. [[CrossRef](#)]
6. Xiong, D.; Liu, X.; Liu, L.; Douthe, C.; Li, Y.; Peng, S.; Huang, J. Rapid responses of mesophyll conductance to changes of CO₂ concentration, temperature and irradiance are affected by N supplements in rice. *Plant Cell Environ.* **2015**, *38*, 2541–2550. [[CrossRef](#)]

7. Teng, S.; Qian, Q.; Zeng, D.; Kunihiro, Y.; Fujimoto, K.; Huang, D.; Zhu, L. QTL analysis of leaf photosynthetic rate and related physiological traits in rice (*Oryza sativa* L.). *Euphytica* **2004**, *135*, 1–7. [[CrossRef](#)]
8. Degl'Innocenti, E.; Guidi, L.; Soldatini, G.F. Effects of elevated ozone on chlorophyll a fluorescence in symptomatic and asymptomatic leaves of two tomato genotypes. *Biol. Plant.* **2007**, *51*, 313–321. [[CrossRef](#)]
9. Li, H.S.; Sun, Q.; Zhao, S.J. *Principles and Techniques of Plant Physiological and Biochemical Experiments*; Higher Education Press: Beijing, China, 2000; pp. 167–169.
10. Griffiths, H.; Weller, G.; Toy, L.; Dennis, R. You're so vein: Bundle sheath physiology, phylogeny and evolution in C₃ and C₄ plants. *Plant Cell Environ.* **2013**, *36*, 249–261. [[CrossRef](#)]
11. Long, S.; Zhu, X.; Naidu, S.; Ort, D. Can improvement in photosynthesis increase crop yield? *Plant Cell Environ.* **2006**, *29*, 315–330. [[CrossRef](#)]
12. Rosenthal, D.M.; Locke, A.M.; Khozaei, M.; Raines, C.A.; Long, S.P.; Ort, D.R. Over-expressing the C₃ photosynthesis cycle enzyme Sedoheptulose-1-7 Bisphosphatase improves photosynthetic carbon gain and yield under fully open air CO₂ fumigation (FACE). *BMC Plant Biol.* **2011**, *11*, 123. [[CrossRef](#)]
13. Takahara, K.; Kasajima, I.; Takahashi, H.; Hashida, S.-N.; Itami, T.; Onodera, H.; Toki, S.; Yanagisawa, S.; Kawai-Yamada, M.; Uchimiya, H. Metabolome and Photochemical Analysis of Rice Plants Overexpressing Arabidopsis NAD Kinase Gene. *Plant Physiol.* **2010**, *152*, 1863–1873. [[CrossRef](#)] [[PubMed](#)]
14. Tholen, D.; Boom, C.; Zhu, X. Opinion: Prospects for improving photosynthesis by altering leaf anatomy. *Plant Sci.* **2012**, *197*, 92–101. [[CrossRef](#)] [[PubMed](#)]
15. Coupe, S.; Palmer, B.; Lake, J.; Overy, S.; Oxborough, K.; Woodward, F.; Gray, J.; Quick, W. Systemic signalling of environmental cues in Arabidopsis leaves. *J. Exp. Bot.* **2006**, *57*, 329–341. [[CrossRef](#)]
16. Giuliani, R.; Koteyeva, N.; Voznesenskaya, E.; Evans, M.A.; Cousins, A.B.; Edwards, G.E. Coordination of Leaf Photosynthesis, Transpiration, and Structural Traits in Rice and Wild Relatives (Genus *Oryza*). *Plant Physiol.* **2013**, *162*, 1632–1651. [[CrossRef](#)]
17. Shunsuke, A.; Toru, N.; Masaki, U.; Kazuya, S.; Toshiyuki, T.; Takao, O.; Toshio, Y.; Taiichiro, O.; Hiroshi, M.; Masahiro, Y. The mesophyll anatomy enhancing CO₂ diffusion is a key trait for improving rice photosynthesis. *J. Exp. Bot.* **2013**, *64*, 1061–1072.
18. Xu, Z.; Zhou, G. Responses of leaf stomatal density to water status and its relationship with photosynthesis in a grass. *J. Exp. Bot.* **2008**, *59*, 3317–3325. [[CrossRef](#)]
19. Ocheltree, T.W.; Nippert, J.; Prasad, P.V. Changes in stomatal conductance along grass blades reflect changes in leaf structure. *Plant Cell Environ.* **2012**, *35*, 1040–1049. [[CrossRef](#)] [[PubMed](#)]
20. Huang, G.; Shu, Y.; Peng, S.; Li, Y. Leaf photosynthesis is positively correlated with xylem and phloem areas in leaf veins in rice (*Oryza sativa*) plants. *Ann. Bot.* **2022**, *129*, 619–631. [[CrossRef](#)]
21. Xiong, D.; Yu, T.; Zhang, T.; Li, Y.; Peng, S.; Huang, J. Leaf hydraulic conductance is coordinated with leaf morpho-anatomical traits and nitrogen status in the genus *Oryza*. *J. Exp. Bot.* **2015**, *66*, 741–748. [[CrossRef](#)]
22. Han, J.; Zhang, Y.; Lei, Z.; Zhang, W. The higher area-based photosynthesis in *Gossypium hirsutum* L. is mostly attributed to higher leaf thickness. *Photosynthetica* **2019**, *57*, 420–427. [[CrossRef](#)]
23. Deng, Y.M.; Li, C.; Shao, Q.; Ye, X.; She, J. Differential responses of double petal and multi petal jasmine to shading: I. Photosynthetic characteristics and chloroplast ultrastructure. *Plant Physiol. Biochem.* **2012**, *55*, 93–102. [[CrossRef](#)] [[PubMed](#)]
24. Wang, X.; Wang, W.; Huang, J.; Peng, S.; Xiong, D. Diffusional conductance to CO₂ is the key limitation to photosynthesis in salt-stressed leaves of rice (*Oryza sativa*). *Physiol. Plant.* **2017**, *163*, 45–58. [[CrossRef](#)] [[PubMed](#)]
25. Huang, D.; Wu, L.; Chen, J.; Dong, L. Morphological plasticity, photosynthesis and chlorophyll fluorescence of *Athyrium pachyphlebium* at different shade levels. *Photosynthetica* **2011**, *49*, 611–618. [[CrossRef](#)]
26. Maxwell, K.; Johnson, G. Chlorophyll fluorescence—A practical guide. *J. Exp. Bot.* **2000**, *51*, 659–668. [[CrossRef](#)]
27. Lande, N.V.; Barua, P.; Gayen, D.; Kumar, S.; Chakraborty, S.; Chakraborty, N. Proteomic dissection of the chloroplast: Moving beyond photosynthesis. *J. Proteom.* **2019**, *212*, 103542. [[CrossRef](#)] [[PubMed](#)]
28. Wang, Y.; Xu, C.; Li, K.; Cai, X.; Wu, M.; Chen, G. Fe deficiency induced changes in rice (*Oryza sativa* L.) thylakoids. *Environ. Sci. Pollut. Res.* **2017**, *24*, 1380–1388. [[CrossRef](#)] [[PubMed](#)]
29. Chen, B.; Wang, Y. Proteomic and Physiological Studies Provide Insight into Photosynthetic Response of Rice (*Oryza sativa* L.) Seedlings to Microgravity. *Photochem. Photobiol.* **2016**, *92*, 561–570. [[CrossRef](#)]
30. Sakataa, S.; Mizusawaa, N.; Kawaib, H.; Sakuraia, I.; Wada, H. Psb28 is involved in recovery of photosystem II at high temperature in *Synechocystis* sp. PCC 6803. *Biochim. Biophys. Acta (BBA)-Bioenerg.* **2013**, *1827*, 50–59. [[CrossRef](#)]
31. Zörb, C.; Herbst, R.; Forreiter, C.; Schubert, S. Short-term effects of salt exposure on the maize chloroplast protein pattern. *Proteomics* **2009**, *9*, 4209–4220. [[CrossRef](#)]
32. Fan, Y.; Chen, J.; Wang, Z.; Tan, T.; Li, S.; Li, J.; Wang, B.; Zhang, J.; Cheng, Y.; Wu, X.; et al. Soybean (*Glycine max* L. Merr.) seedlings response to shading: Leaf structure, photosynthesis and proteomic analysis. *BMC Plant Biol.* **2019**, *19*, 34. [[CrossRef](#)] [[PubMed](#)]
33. He, L.; Li, M.; Qiu, Z.; Chen, D.; Zhang, G.; Wang, X.; Chen, G.; Hu, J.; Gao, Z.; Dong, G.; et al. Primary leaf-type ferredoxin 1 participates in photosynthetic electron transport and carbon assimilation in rice. *Plant J.* **2020**, *104*, 44–58. [[CrossRef](#)] [[PubMed](#)]
34. Feng, D. Photosynthetic Characteristics and Quantitative Proteomics Analysis of Maize and Rice Leaves. Ph.D. Thesis, Chinese Academy of Agricultural Sciences, Beijing, China, 2007.

35. Zhang, Z.; Mao, X.; Ou, J.; Ye, N.; Zhang, J.; Peng, X. Distinct photo respiratory reactions are preferentially catalyzed by glutamate: Glyoxylate and serine: Glyoxylate aminotransferases in rice. *J. Photochem. Photobiol. B Biol.* **2015**, *142*, 110–117. [[CrossRef](#)] [[PubMed](#)]
36. Imaizumi, N.; Samejima, M.; Ishihara, K. Characteristics of photosynthetic carbon metabolism of spikelets in rice. *Photosynth. Res.* **1997**, *52*, 75–82. [[CrossRef](#)]
37. Agarie, S.; Miura, A.; Sumikura, R.; Tsukamoto, S.; Nose, A.; Arima, S.; Matsuoka, M.; Miyao-Tokutomi, M. Overexpression of C₄ PEPC caused O₂-insensitive photosynthesis in transgenic rice plant. *Plant Sci.* **2002**, *162*, 257–265. [[CrossRef](#)]
38. Fukayama, H.; Hatch, M.D.; Tamai, T.; Tsuchida, H.; Sudoh, S.; Furbank, R.T.; Miyao, M. Activity regulation and physiological impacts of maize C₄-specific phosphoenolpyruvate carboxylase overproduced in transgenic rice plants. *Photosyn Res.* **2003**, *77*, 227–239. [[CrossRef](#)]
39. Ku, M.S.; Agarie, S.; Nomura, M.; Fukayama, H.; Tsuchida, H.; Ono, K.; Hirose, S.; Toki, S.; Miyao, M.; Matsuoka, M. High-level expression of maize phosphoenolpyruvate carboxylase in transgenic rice plants. *Nat. Biotechnol.* **1999**, *17*, 76–80. [[CrossRef](#)]